Cascade Control Solutions for Maglev Systems

Elena-Lorena Hedrea
AAI Department
Politehnica Univ. Timisoara
Timisoara, Romania
elena.constantin@student.upt.ro

Radu-Emil Precup
AAI Department
Politehnica Univ. Timisoara
Timisoara, Romania
radu.precup@upt.ro

Claudia-Adina Bojan-Dragos
AAI Department
Politehnica Univ. Timisoara
Timisoara, Romania
claudia.dragos@aut.upt.ro

Raul-Cristian Roman
AAI Department
Politehnica Univ. Timisoara
Timisoara, Romania
raul-cristian.roman@student.upt.ro

Oana Tanasoiu
AAI Department
Politehnica Univ. Timisoara
Timisoara, Romania
oanatanasoiu96@gmail.com

Marius Marinescu
AAI Department
Politehnica Univ. Timisoara
Timisoara, Romania
mariusmarinescu185@gmail.com

***Abstract*—In this paper a cascade control system (CCS) structure made of a combination of tensor product (TP)-based model transformation and of fuzzy control is designed for the position control of the magnetic levitation (Maglev) laboratory equipment. The linearized Maglev system model was first stabilized using two control method: a state-feedback control structure (SF-CS) and a Proportional-Integral-state feedback control structure (PISF-CS). A comparative study of these state-feedback CSs is also included. A parallel distributed compensation technique (PDC) is used in the TP-based design of the inner state feedback control loops which was next simplified by simple least squares identification algorithms. In the next step the Takagi-Sugeno (TS) fuzzy controller is designed in the outer control loops using the modulus optimum method and the modal equivalence principle. A comparative analysis and experimental results are given to validate the efficiency of the proposed CCS structure.**

Keywords— cascade control system structure; TP–based model transformation; fuzzy control; experimental results; Maglev systems

I. INTRODUCTION

The magnetic levitation (Maglev) system is a nonlinear and unstable laboratory equipment used in many practical applications.

The next short bibliographic list contains some recent control structure (CS) design approaches for the Maglev system given in the literature. This list includes: a Proportional-Integral (PI)-state feedback controller and Proportional-Derivative (PD) controllers [1], (Inteco, 2008), neural networks-based controller [2], state observers (Lee et al., 2007), both flux and current feedback controllers (Fan et al., 2014), a fault-tolerant controller (Zhai et al., 2017), an adaptive robust sliding mode controller and a vibration filter controller in [3], a fractional order PID controller in [4], a PD and a Proportional-Integral-Derivative (PID) controller in [5], Linear-Quadratic-Gaussian control in [6]. Many types of fuzzy controllers were applied to Maglev systems as: a hybrid fuzzy decoupling controller in [7], a fuzzy PI controller based on feedback linearization in (Hu et al., 2011), a fuzzy sliding mode control based of feedback linearization in (Yu et al., 2010), a back stepping fuzzy-neural-network controller in (Wai et al., 2014) and (Wai et al, 2015), a discrete switched fuzzy controller in (Mahmoud et al, 2015).

The Tensor Product–based model transformation (TP–MT) is a numerical method, which starts with Linear Parameter–Varying (LPV) dynamic models and produces Linear Time-Invariant (LTI) systems. The main advantage of this technique is that both the linear matrix inequality (LMI) and the parallel distributed compensation (PDC) frameworks are applied immediately to the affine models. The generalized TP–MT is proposed in [8] along with an analysis on how it can be used both in modeling and in polytopic model-based design approaches. In [9] the TP-MT is used in order to obtain polytopic quasi– Linear Parameter–Varying (qLPV) models of diabetes mellitus. TP-based control schemes with friction compensation are proposed in [10]–[12]. Electric drive and temperature control applications are given in [13] and [14]. The stabilization of a 3-degrees of freedom (DOF) remote control (RC) helicopter via the combination of TP and PDC is carried out in [15]. The TP model transformation is also used for position control of a Maglev system in [16] and for the water level control of a vertical three tank systems in [17].

Other combinations of TP–MT and PI and fuzzy control as a cascade control system structure are presented in [14], [18], [19]. These CS combinations were validated by laboratory equipment such as horizontal three tank systems, vertical three tank systems and Air Stream and Temperature Control Plant (ASTCP).

The main contribution of this paper is the design and real-time validation of two cascade control structures (CCS) for the position control of a Maglev laboratory equipment. The linearized Maglev system model is stabilized in the first step using two control methods: a state-feedback control structure (SF-CS) and a PI-state feedback control structure (PISF-CS). In the second step, one CCS which consists of an inner TP-based state feedback control loop (TP-SF-CS) and an outer Tagaki–Sugeno (TS) fuzzy controller-based control loop

This work was supported by a grant of the Politehnica University of Timisoara, Romania, project number PCD-TC-UPT-2017.

(fuzzy-TP-SF-CS) is designed for SF-CS and one CCS which consists of an inner TP-based PI state feedback control loop (TP-PISF-CS) and outer TS fuzzy controller-based control loop (fuzzy-TP-SF-CS) is designed for PISF-CS. A PDC technique is used in TP-SF-CS and TP-PISF-CS respectively which were next characterized by benchmark type simplified models. The modulus optimum method (MO-m) and the modal equivalent principle are used in the second step to design the fuzzy-TP-SF-CS and fuzzy-TP-PISF-CS respectively. The experimental validation of the CCS for the stabilized linearized Maglev system model. The comparison of two types of CSs for the Maglev system: the SF-CS proposed in this paper and the PISF-CS discussed in [1]. Both structures involve control algorithms with similar complexity, namely fuzzy and state feedback ones.

The paper treats these topics: the stabilization of the Maglev system is given in Section II. Section III is dedicated to the design of the two cascade CS for the stabilized linearized Maglev system model. The experimental results and the control performances are presented in Section IV. The conclusions are pointed out in Section V.

II. Stabilization of Maglev System. Comparative Study

The state–space process model of Maglev system is (Inteco, 2008)

$$\begin{aligned}
&\dot{x}_1(t) = v(t),\\
&\dot{v}(t) = -\frac{i_{EM1}^2(t)\cdot F_{emP1}\cdot \exp[-x_1(t)/F_{emP2}]}{m\cdot F_{emP2}} + g\\
&\qquad + \frac{i_{EM2}^2(t)\cdot F_{emP1}\cdot \exp[-(x_d - x_1(t))]/F_{emP2}}{m\cdot F_{emP2}},\\
&\dot{i}_{EM1}(t) = \frac{k_i\cdot u_{EM1}(t) + c_i - i_{EM1}(t)}{(f_{iP1}/f_{iP2})\cdot \exp[-x_1(t)/f_{iP2}]},\\
&\dot{i}_{EM2}(t) = \frac{k_i\cdot u_{EM2}(t) + c_i - i_{EM2}(t)}{(f_{iP1}/f_{iP2})\cdot \exp[-(x_d - x_1(t))/f_{iP2}]},\\
&y(t) = k_m\cdot x_1(t),
\end{aligned} \tag{1}$$

where: $x_1 \in [0, 0.0016]$ – the sphere position (m), $v \in \Re$ – the sphere speed (m/s), i_{EM1}, $i_{EM2} \in [0.03884, 2.38]$ – the currents in the upper electromagnet (EM1) and lower electromagnet (EM2) (A), u_{EM1}, $u_{EM2} \in [0.005, 1]$ – the (control and/or disturbance) signals applied to EM1 and EM2, respectively (V), and y – the controlled output (m). The parameters of this process (Inteco, 2008), (Bojan-Dragos et al., 2016) get the following values: D_s=0.06 (m) is the diameter of the sphere, x_d =0.09 (m) is the distance between electromagnets minus sphere diameter, g=9.81 (m/s^2) is the gravity acceleration, m=0.0571 (kg) is the sphere mass, the parameters k_i=0.0243 (A) and c_i=2.5165 (A) correspond the actuator dynamic analysis, F_{emP1}=1.7521·10^{-2} (H), F_{emP2}=5.8231·10^{-3} (m), f_{iP1}=1.4142·10^{-4} (ms), f_{iP2}=4.5626·10^{-3} (m).

In order to design the proposed CSs, the model (1) is first reduced from a fourth–order system to a third–order system with the following state variables: the position x_1, the speed v and the current in EM1, i_{EM1}. Then the reduced model is linearized at an equilibrium point (Inteco, 2008) with the coordinates $P(x_1, v, i_{EM1}, u_{EM1})$:

$$\begin{aligned}
&\begin{cases}\dot{\mathbf{x}} = \mathbf{A}\,\mathbf{x} + \mathbf{b}_{u1}u_1\\ y = \mathbf{c}^T\mathbf{x}\end{cases},\\
&\mathbf{x} = [x_1 \quad v \quad i_{EM1}]^T,\ \mathbf{x}\in\Re^{3x1},\ u_1\in\Re,\ y = x_1,
\end{aligned} \tag{2}$$

where the elements of the matrices $\mathbf{A}$ and $\mathbf{b}_{u1}$ are

$$\begin{aligned}
&\mathbf{A} = \begin{bmatrix} 0 & 1 & 0\\ a_{21} & 0 & a_{23}\\ a_{31} & 0 & a_{33}\end{bmatrix},\ \mathbf{b}_{u1} = \begin{bmatrix} 0\\ 0\\ b_{31}\end{bmatrix},\\
&\mathbf{c}^T = [1 \quad 0 \quad 0],\ \mathbf{A}\in\Re^{3x3},\ \mathbf{b}_{u1}\in\Re^{3x1},\ \mathbf{c}^T\in\Re^{1x3},
\end{aligned} \tag{3}$$

and their full expressions are given in (Bojan-Dragos et al., 2016) and [20].

The linearized model (2) is stabilized by state feedback and pole placement control design (Bojan-Dragos et al., 2016) and [20], with the imposed closed–loop system poles $p^* = \{-31.81, -41.05, -231.94\}$, and the gain matrix $\mathbf{k}_c^T = [66.63 \quad 1.62 \quad -0.15]$ is obtained. The resulted state–space model of the stabilized linearized Maglev control system (SF-CS) model is:

$$\begin{aligned}
&\dot{\mathbf{x}} = \mathbf{A}_x\,\mathbf{x} + \mathbf{b}_{1x}\,u_{1x},\ \mathbf{x}\in\Re^{1x3}\\
&y = \mathbf{c}^T\mathbf{x},\\
&\mathbf{A}_x = \begin{bmatrix} 0 & 1 & 0\\ a_{21} & 0 & a_{23}\\ a_{31} & a_{32} & a_{33}\end{bmatrix},\ \mathbf{b}_{1x} = \begin{bmatrix} 0\\ 0\\ b_{31}\end{bmatrix},\\
&\mathbf{c}^T = [1\ 0\ 0],\ \mathbf{x} = [x_1 \ \ v \ \ i_{EM1}]^T,\\
&\mathbf{A}_x\in\Re^{3x3},\ \mathbf{b}_{1x}\in\Re^{3x1},\ \mathbf{c}^T\in\Re^{1x3},\ u_{1x}\in\Re,
\end{aligned} \tag{4}$$

where the elements of the matrices $\mathbf{A}_x$ and $\mathbf{b}_{1x}$ are given in (Bojan-Dragos et al., 2016) and [20], and T indicates matrix transposition. The block diagram of SF-CS is given in Fig. 1 (a).

In order to compare the SF-CS designed by the authors, a similar CS with PI state-feedback controller, namely PISF-CS, was designed following the steps presented in [1]. The block diagram is illustrated in Fig. 1 (b).

The control law of the PISF-CS is

$$u_{1x} = \mathbf{k}_P\mathbf{x} + \mathbf{k}_I\int\mathbf{x}(\tau)d\tau, \tag{5}$$

where $\mathbf{k}_P$ and $\mathbf{k}_I$ are the PI state feedback gain matrices, namely row matrices for this CS.

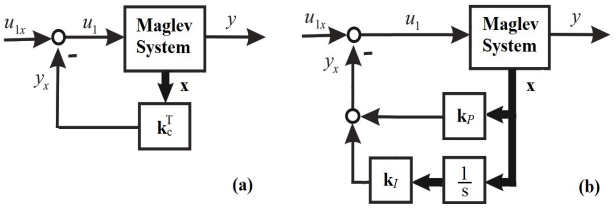

Fig. 1. Block diagram of SF-CS (a) and PISF–CS (b) for Maglev.

The state equation of the obtained PISF-CS closed-loop system model is

$$\dot{\mathbf{x}} = (\mathbf{A} + \mathbf{b}_{u1}\mathbf{k}_P)\mathbf{x} + \mathbf{b}_{u1}\mathbf{k}_I \int_0^t \mathbf{x}(\tau)d\tau. \tag{6}$$

In order to compute the gain matrices $\mathbf{k}_P$ and $\mathbf{k}_I$, the closed-loop characteristic equation (7) and the desired characteristic polynomial (8) are used:

$$\det[s\mathbf{I} - (\mathbf{A} + \mathbf{b}_{u1}\mathbf{k}_P) - \mathbf{b}_{u1}\mathbf{k}_I / s] = 0, \tag{7}$$

$$\Delta_d(s) = \beta_0 + \beta_1 s + ... + \beta_n s^n + \beta_{n+1} s^{n+1}. \tag{8}$$

Using the linearized model (2) and imposing the same closed loop poles as in SF-CS case, the following values of the PISF-CS gain matrices were obtained: $\mathbf{k}_P = [65.13 \quad 1.76 \quad -0.21]$, $\mathbf{k}_I = [25.13 \quad 1.04 \quad -0.2]$.

III. The Cascade Control Structures Design

The design of the CSs presented in the following paragraphs are treated in an unified manner for both the SF-CS and PISF-CS, namely TP-SF-CS, TP-PISF-CS, fuzzy-TP-SF-CS and fuzzy-TP-PISF-CS. In order to present the numerical values of the controller tuning parameters the authors have used the following superscript: (1) for SF-CS and (2) for PISF-CS. The design approach applied to the CCS structure consists of the design of the TP-based Controller and the design of the TS fuzzy controller.

A. The TP-based Controller Design

The main idea of TP–MT was originally introduced in [8]. The TP–MT converts LPV dynamic models into convex combinations of LTI systems using the LMI-based control design techniques in order to satisfy the CS performance requirements. These combinations depend on variable parameters, which can also be important variables of the control systems as, for example, a part of the state variables.

In this paper two TP-based CSs, namely TP-SF-CS and TP-PISF-CS, were designed for both the SF-CS and the PISF-CS using the block diagram given in Fig. 2, where *ref* is the reference input (the set-point).

The TP–MT consists of three steps, which are given in more detail in [8], [21] and [22].

Let the following qLPV model [8]:

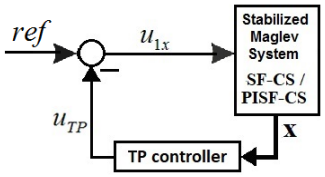

Fig. 2. Block diagram of TP–SF–CS / TP-PISF-CS for Maglev system, where "Stabilized" indicates that the linearized process model given in (3) is actually stabilized.

$$\begin{aligned} \dot{\mathbf{x}}(t) &= \mathbf{A}(\mathbf{p}(t))\mathbf{x}(t) + \mathbf{B}(\mathbf{p}(t))\mathbf{u}(t), \\ \mathbf{y}(t) &= \mathbf{C}(\mathbf{p}(t))\mathbf{x}(t) + \mathbf{D}(\mathbf{p}(t))\mathbf{u}(t), \end{aligned} \tag{9}$$

with input $\mathbf{u}(t) \in \Re^m$, output $\mathbf{y}(t) \in \Re^l$ and state vector $\mathbf{x}(t) \in \Re^q$. The parameter vector fulfils

$$\mathbf{p}(t) \in \Omega, \ \Omega = [a_1, b_1] \times [a_2, b_2] \times ... \times [a_N, b_N] \subset \Re^N, \tag{10}$$

where Ω is a closed hypercube. The system matrix

$$\mathbf{S}(\mathbf{p}(t)) = \begin{pmatrix} \mathbf{A}(\mathbf{p}(t)) & \mathbf{B}(\mathbf{p}(t)) \\ \mathbf{C}(\mathbf{p}(t)) & \mathbf{D}(\mathbf{p}(t)) \end{pmatrix} \in \Re^{(l+q)\times(m+q)} \tag{11}$$

is a parameter–varying object.

For any parameter vector $\mathbf{p}(t)$ the system matrix $\mathbf{S}(\mathbf{p}(t))$ in (11) is given as:

$$\mathbf{S}(\mathbf{p}(t)) = \mathbf{S} \overset{N}{\underset{n=1}{\otimes}} \mathbf{w}(p_n(t)) \tag{12}$$

where $\mathbf{S}_{i_1, i_2, ..., i_N}$ are the LTI vertex systems, $\mathbf{w}(p_n(t))$ are the weighting function (w.f.) matrices, *m* is the number of system inputs, and *q* is the number of state variables [16], [21].

The stabilized linearized Maglev system model for both SF-CS and PISF-CS can also be expressed as:

$$\begin{aligned} \dot{\mathbf{x}} &= \mathbf{A}_x(\mathbf{p})\mathbf{x} + \mathbf{b}_{1x}(\mathbf{p})u_{1x}, \\ y &= \mathbf{c}^T(\mathbf{p})\mathbf{x}, \end{aligned} \tag{13}$$

where $\mathbf{x} = [x_1 \quad v \quad i_{EM1}]^T$ is the process state vector, $\mathbf{p(t)} = [p_1 \quad p_2]^T = [x_1 \quad i_{EM1}]^T$ is the bounded parameter vector, y is, as in Section II, the controlled output, the matrices $\mathbf{A}_x(\mathbf{p}), \mathbf{b}_{1x}(\mathbf{p}), \mathbf{c}^T(\mathbf{p})$ result from (Bojan-Dragos et al. 2016), and *T* points out matrix transposition.

Introducing in (13) the following notation:

$$\mathbf{S}(\mathbf{p}) = [\mathbf{A}_x(\mathbf{p}) \quad \mathbf{b}_{1x}(\mathbf{p})] \in \Re^{3\times4}, \tag{14}$$

the model is transformed in the qLPV state–space form

$$\dot{\mathbf{x}} = \mathbf{S}(\mathbf{p})[\mathbf{x}^T \quad u_{1x}]^T, \qquad y = \mathbf{c}^T(\mathbf{p})\mathbf{x}. \tag{15}$$

Using (12) and (15), the idea of TP–MT is to obtain LTI models from the qLPV model (15) as follows:

$$\begin{aligned}\dot{\mathbf{x}} &= \mathbf{S}(\mathbf{p}(t))[\mathbf{x}^T \quad u_{1x}]^T = \mathbf{S}(\mathbf{p}) \overset{N}{\underset{n=1}{\otimes}} \mathbf{w}_n(\mathbf{p}_n)[\mathbf{x}^T \quad u_{1x}]^T \\ &= \sum_{i=1}^{I}\sum_{k=1}^{K} w_{1,i}(p_1) w_{2,k}(p_2)\mathbf{S}_{i,k}[\mathbf{x}^T \quad u_{1x}]^T, \\ y &= \mathbf{c}^T(\mathbf{p})\mathbf{x},\end{aligned} \tag{16}$$

where $\mathbf{S}$ is the $(N+2)$−dimensional core tensor, $\mathbf{w}_n(\mathbf{p}_n)$ are the continuous w.f. matrices, N is tensor's dimension, i and k are the numbers of singular values for position and current, respectively. The w.f.s in this paper are of CNO type.

The resulted stabilized linearized Maglev system LTI models are obtained for three singular values for position, $i = 1...3$, and three singular values for current, $k = 1...3$:

$$\dot{\mathbf{x}} = \sum_{i=1}^{3}\sum_{k=1}^{3} w_{1,i}(p_1) w_{2,k}(p_2)(\mathbf{A}_{xi,k}\mathbf{x} + \mathbf{b}_{1xi,k}u_{1x}) \qquad y = \mathbf{c}^T(\mathbf{p})\mathbf{x} \tag{17}$$

Two control objectives are imposed: the first one is to carry out the asymptotic stabilization of the control system and the second one is to constrain the control signal. The first control objective is solved by the application of the PDC design framework. The asymptotic stability of the closed-loop CS is equivalent to the sufficient condition of existence of $\mathbf{X} = \mathbf{P}^{-1} > 0$ (with $\mathbf{P}$ – a positive definite regular matrix) and $\mathbf{M}_{i,k}$ that satisfy the following LMIs [8], [21]:

$$\begin{aligned}&-\mathbf{X}\mathbf{A}_{xi,k}^T - \mathbf{A}_{xi,k}\mathbf{X} + \mathbf{M}_{i,k}^T\mathbf{X}_{i,k}^T + \mathbf{b}_{1xi,k}\mathbf{M}_{i,k} > 0, \\ &-\mathbf{X}\mathbf{A}_{xi,k}^T - \mathbf{A}_{xi,k}\mathbf{X} - \mathbf{X}\mathbf{A}_s^T - \mathbf{A}_s\mathbf{X} + \mathbf{M}_s^T\mathbf{b}_{1xi,k}^T \\ &+ \mathbf{b}_{1xi,k}\mathbf{M}_s + \mathbf{M}_{i,k}^T\mathbf{B}_s^T + \mathbf{B}_s\mathbf{M}_{i,k} \geq 0,\ i = 1...3,\ k = 1...3.\end{aligned} \tag{18}$$

The state feedback gain matrices $\mathbf{K}_{i,k}$ that corresponds to each LTI vertex system are next computed as [21]

$$\mathbf{K}_{i,k} = \mathbf{M}_{i,k}\mathbf{X}^{-1}. \tag{19}$$

After that, the application of PDC to the stabilized linearized Maglev system model leads to the state feedback control law:

$$u_{1x} = ref - u_{TP} = ref - \left[\sum_{i=1}^{3}\sum_{k=1}^{3} w_{1,i}(p_1) w_{2,k}(p_2)\mathbf{K}_{i,k}\right]\mathbf{x}, \tag{20}$$

In order to solve the second control objective, it is assumed that $\| \mathbf{x}(0) \|_2 \leq \phi$, where $\mathbf{x}(0) = [0 \quad 0 \quad 0]^T$, and $\phi = 1.1 > 0$. Then the following LMI results [21]:

$$\phi^2\mathbf{I} \leq \mathbf{X}. \tag{21}$$

The constraint $|u_{1x}| \leq \mu$ ($\mu = 10$ in this paper) is applied at all time moments if the next nine LMIs are satisfied:

$$\begin{pmatrix} \mathbf{X} & \mathbf{M}_{i,k}^T \\ \mathbf{M}_{i,k} & \mu^2\mathbf{I} \end{pmatrix} \geq 0,\ i = 1...3,\ k = 1...3. \tag{22}$$

The matrices $\mathbf{X}$ and $\mathbf{M}_{i,k}$ are computed by solving the stability conditions (18), (21) and (22) using the YalmipR2015 solver [16]. The solutions are next substituted in (19) leading to the values of the LTI feedback gains.

Examples of feedback gains $\mathbf{K}_{i,k}^{(1)}$ obtained for SF-CS are $\mathbf{K}_{1,1}^{(1)} = [-271.49 \ \ 1.87 \ \ -1.22]$, $\mathbf{K}_{3,3}^{(1)} = [-322.79 \ \ 1.87 \ \ -1.08]$, and the ones obtained for PISF-CS, $\mathbf{K}_{i,k}^{(2)}$ are $\mathbf{K}_{1,1}^{(2)} = [-265.01 \ \ 1.32 \ \ -1.45]$, $\mathbf{K}_{3,3}^{(2)} = [-315.84 \ \ 1.03 \ \ -1.67]$.

The equivalent state feedback gain matrices given above are employed in the computation of the following two three-order benchmark type closed-loop transfer functions of the inner control loops, $H_P^{(1)}(s)$ and $H_P^{(2)}(s)$:

$$H_P^{(1)}(s) = k_P^{(1)}/[(1+T_1^{(1)}s)(1+T_2^{(1)}s)(1+T_3^{(1)}s)], \tag{25}$$

$$H_P^{(2)} = k_P^{(2)}/[(1+T_1^{(2)}s)(1+T_2^{(2)}s)(1+T_3^{(2)}s)], \tag{26}$$

where $k_P^{(1)} = 1.02, k_P^{(2)} = 0.89$ are the controlled process gains, $T_1^{(1)} = 0.1, T_1^{(2)} = 0.068$ are the large time constants, $T_2^{(1)} = 0.03, T_3^{(1)} = 0.009, T_2^{(2)} = 0.048, T_3^{(2)} = 0.012$ are the small time constants. Using a simple least-squares-based experimental approximation of the inner control loops the above parameters were obtained.

The third order t.f.s. (25) and (26) were reduced to second order benchmark type closed-loop t.f. and two PI controllers were designed using MO-m with the general t.f.:

$$H_{PI}(s) = k_c(1 + sT_c)/s. \tag{27}$$

The following numerical values of PI controller tuning parameters $k_c^{(1)} = 1/(2 \cdot k_P^{(1)} \cdot T_\Sigma^{(1)}) = 12.25$, $T_\Sigma^{(1)} = T_2^{(1)} + T_3^{(1)}$ and $T_c^{(1)} = T_1^{(1)} = 0.1$ are obtained for SF-CS and $k_c^{(2)} = 1/(2 \cdot k_P^{(2)} \cdot T_\Sigma^{(2)}) = 9.36$, $T_\Sigma^{(2)} = T_2^{(2)} + T_3^{(2)}$ and $T_c^{(2)} = T_1^{(2)} = 0.068$ are obtained for PISF-CS.

B. The Takagi-Sugeno Fuzzy Controller Design

The improvement of the CS performance is obtained by the replacement of the PI controller in the outer loops with the t.f. (26) by TS fuzzy controllers. The two control structures, namely fuzzy-TP-SF-CS / fuzzy-TP-PISF-CS are obtained with the block diagram illustrated in Fig. 3.

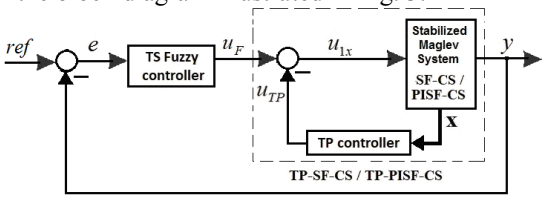

Fig. 3. Block diagram of CCS for the stabilized linearized Maglev system model.

The fuzzy controller design is formulated from the PI controller design as the fuzzy controllers considered in this paper are carrying out the nonlinear merge of seven linear PI controllers placed in the rule consequents. Tustin's method with $T_s = 0.00025$ s was used in order to discretize the continuous-time PI controllers. The quasi-continuous digital PI controller is obtained as:

$$\Delta u_F^{(r)}(k) = \gamma^{(r)}[\alpha^{(r)} K_P e(k) + K_I \Delta e(k)], \tag{28}$$

where $r = \overline{1,7}$ is the index of the controller used in the consequent of the rules of the TS fuzzy controller; the big number of the values for index *r* (seven) was chosen in order to ensure a smooth and continuous switching between the PI controllers and an appropriate nonlinear input-output map of the TS fuzzy controller; T_s is the sampling period and the expressions of the PI controller tuning parameters, K_P and K_I are

$$K_P = 1 - T_s/(2T_c),\ K_I = T_s/T_c. \tag{29}$$

The fuzzification employs five linguistic terms with triangular and trapezoidal membership functions for the input variables, $e(k)$ and $\Delta e(k)$.

The parameters of fuzzy block $B_e > 0$ and $B_{\Delta e}$ are chosen based on the experience of the CS designer and on modal equivalence principle. MAX-MIN compositional rule of inference is used in the inference engine. The center of gravity method is used for defuzzification.

The rule base of the discrete-time dynamic TS fuzzy model consists of 25 fuzzy rules

$$\begin{aligned} &\text{IF } (e(k) \text{ IS LT}_{\text{e}} \text{ AND } \Delta e(k) \text{ IS LT}_{\Delta \text{e}}) \text{ THEN} \\ &\Delta u_F^{(r)}(k) = \gamma^{(r)}[\alpha^{(r)} K_P e(k) + K_I \Delta e(k)], \end{aligned} \tag{30}$$

which are also given in Table I. This rule base is used in both cases SF-CS and PISF-CS.

The appropriate choosing of the values of the parameters $\eta > 0$ and $\alpha > 0$ can modify the control system performance indices. In the experimental scenario, the numerical values of these parameters are: $B_e^{(1)} = 0.02$, $\gamma^{(1)} \in \{3,\ 4,\ 4.6,\ 2.4,\ 1.75,\ 3.3,\ 4.5\}$ and $\alpha^{(1)} \in \{0.01,\ 0.0087,\ 0.007,\ 0.005,\ 0.0032,\ 0.0031,\ 0.0033\}$ for TP-SF-CS and $B_e^{(2)} = 0.017$, $\gamma^{(2)} \in \{3.5,\ 4.1,\ 5,\ 2.6,\ 2,\ 3.8,\ 4.9\}$, and $\alpha^{(2)} \in \{0.012, 0.009, 0.0076,\ 0.0054, 0.003, 0.0029, 0.0038\}$ for TP-PISF-CS.

TABLE I. THE RULE BASE

$\Delta e(k)$	$e(k)$				
	NB	NS	ZE	PS	PB
PB	$\Delta u_F^{(4)}$	$\Delta u_F^{(5)}$	$\Delta u_F^{(6)}$	$\Delta u_F^{(7)}$	$\Delta u_F^{(7)}$
PS	$\Delta u_F^{(3)}$	$\Delta u_F^{(4)}$	$\Delta u_F^{(5)}$	$\Delta u_F^{(6)}$	$\Delta u_F^{(7)}$
ZE	$\Delta u_F^{(2)}$	$\Delta u_F^{(3)}$	$\Delta u_F^{(4)}$	$\Delta u_F^{(5)}$	$\Delta u_F^{(6)}$
NS	$\Delta u_F^{(1)}$	$\Delta u_F^{(2)}$	$\Delta u_F^{(3)}$	$\Delta u_F^{(4)}$	$\Delta u_F^{(5)}$
NB	$\Delta u_F^{(1)}$	$\Delta u_F^{(1)}$	$\Delta u_F^{(2)}$	$\Delta u_F^{(3)}$	$\Delta u_F^{(4)}$

The control signal applied to the u_{1x} is computed by combining output variable of the TP controller, u_{TP}, with the output variable of the TS fuzzy control, u_F, as

$$u_{1x} = u_F - u_{TP}, \tag{31}$$

where u_{TP} is given in (20) and u_F is the control signal applied to TP-SF-CS and is obtained after the integration of Δu_F according to

$$u_F(k) = \Delta u_F(k) + u_F(k-1). \tag{32}$$

However, equation (32) is not needed if an integral process (including the actuator) is controlled. PD fuzzy controllers are used in such situations, and Δu_F is applied directly to the actuator.

IV. EXPERIMENTAL RESULTS

This section is dedicated to test, analyze and validate the proposed CSs by real-time experimental results plotted in Figs. 4 to 8. First of all, all CSs were tested on the time frame of 20 s using a step reference input of 0.007 m amplitude. Only the sphere position vs. time is plotted for all CSs. For the comparative analysis three pairs of CSs were taken into consideration: {SF-CS and PISF-CS}, {TP-SF-CS and TP-PISF-CS} and {fuzzy-TP-SF-CS and fuzzy-TP-PISF-CS}.

The first two CSs used to stabilize the linearized Maglev system model, SF-CS and PISF-CS, are plotted in Fig. 4. The TP-SF-CS and TP-PISF-CS were also tested on the real-world Maglev system and the responses of sphere position are illustrated in Fig. 5. The fuzzy-TP-SF-CS and fuzzy-TP-PISF-CS were tested on the Maglev system in three testing scenarios: (i) on step reference the resulted sphere position is presented in Fig. 6; (ii) a sine reference input was applied to the CCSs and the resulted sphere position is presented in Fig. 7; (iii) a staircase reference input signal was applied to the CCSs and the resulted sphere position is presented in Fig. 8.

In Table II and Table III, the performance indices in terms of mean square error (MSE), settling time and overshoot are highlighted and best results achieved are marked with "X". The

best performance in terms of MSE was achieved by the fuzzy-TP-SF-CS for all three reference input cases. The best performance in terms of overshoot is achieved by the fuzzy-TP-SF-CS for staircase reference input case.

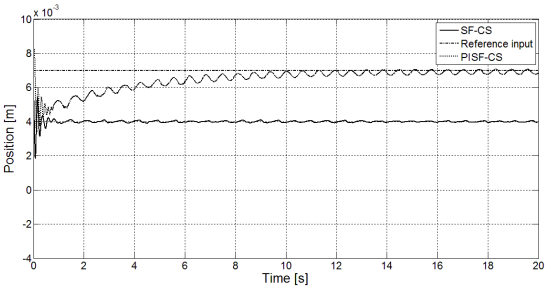

Fig. 4. Sphere position x_1 vs. time for SF-CS and PISF-CS with step reference input.

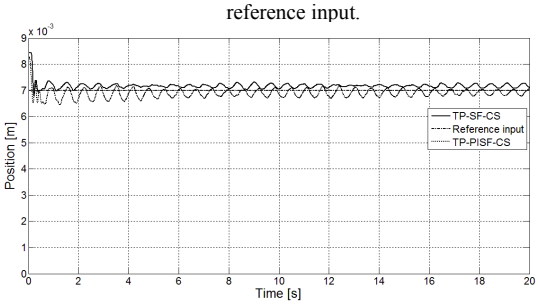

Fig. 5. Sphere position x_1 vs. time for TP-SF-CS and TP-PISF-CS with step reference input.

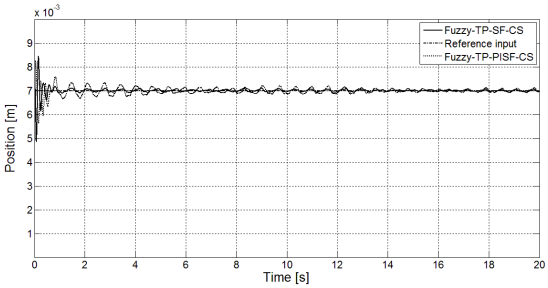

Fig. 6. Sphere position x_1 vs. time for Fuzzy-TP-SF-CS and Fuzzy-TP-PISF-CS with step reference input.

In all three cases namely PISF-CS, TP-PISF-CS and fuzzy-TP-PISF-CS, the zero steady-state control error is ensured due to the presence of the integrator in the SF structure, which is an advantage compared to CS proposed by the authors, SF-CS. These CSs have the following disadvantage: the settling time is bigger than the one computed in the CS designed by authors and there are many oscillations.

The experimental results indicate that CSs with several controllers track the reference of the position of the sphere. Although the objectives of this TP controller are to carry out the asymptotic stabilization of the control system and to restrict the control signal, so it is not the purpose of this controller to track a reference input, the integrator deals with reference input tracking.

TABLE II. MEAN SQUARE ERROR

Control structures	Step reference input			Compara-tive analysis
	MSE (m)	Settling time (s)	Over shoot (%)	
SF-CS	$9.03 \cdot 10^{-6}$	-	-	
PISF-CS	$6.73 \cdot 10^{-7}$	12	-	X
TP-SF-CS	$4.93 \cdot 10^{-8}$	6	21	
TP-PISF-CS	$4.39 \cdot 10^{-8}$	6	15	X
Fuzzy-TP-SF-CS	$2.16 \cdot 10^{-8}$	4	21	X
Fuzzy-TP-PISF-CS	$3.1 \cdot 10^{-8}$	13	18	

V. CONCLUSION

This paper has presented the design and real-time validation of two CCSs applied to Maglev system position control systems. The linearized Maglev system model was stabilized using a state-feedback CS and a PI-state feedback CS. Then, for each CS two cascade control structures were designed consisting in a combination of TP–MT and fuzzy control. The real time experimental results prove that the CCS structure with fuzzy-TP-SF-CS ensures zero steady–state control error, small settling times and overshoots. The values of MSE are small due to the fact that the order of magnitude of the reference input and the controlled output (the sphere position) is millimeters.

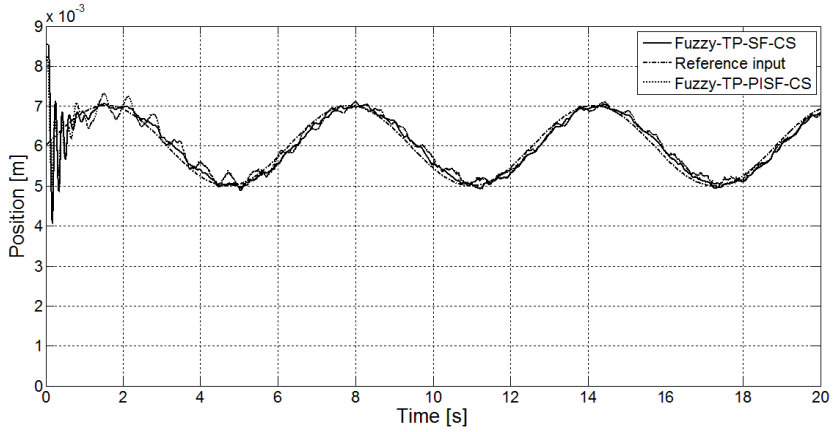

Fig. 7. Sphere position x_1 vs. time for Fuzzy-TP-SF-CS and Fuzzy-TP-PISF-CS with sine reference input.

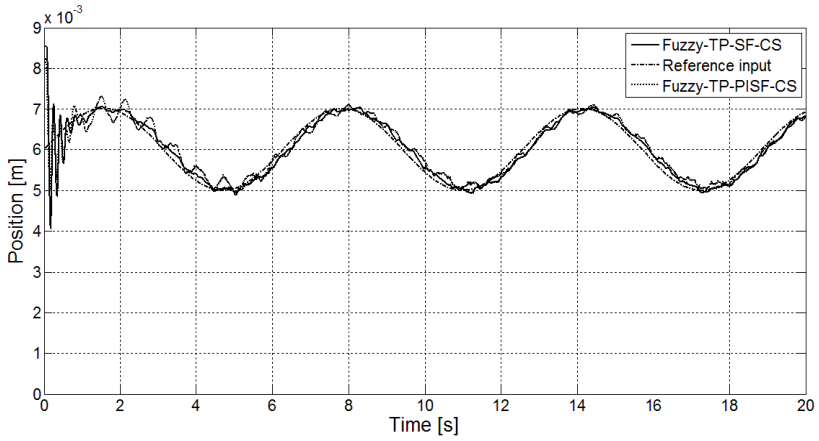

Fig. 8. Sphere position x_1 vs. time for Fuzzy-TP-SF-CS and Fuzzy-TP-PISF-CS with staircase reference input.

TABLE III. PERFORMANCE INDICES

Control structure	Sine reference input	Staircase type reference input						Comparative analysis
	MSE (m)	MSE (m)	Settling time (s)			Overshoot (%)		
			R1	R2	R3	R1	R2	R3	
Fuzzy-TP-SF-CS	$5.7 \cdot 10^{-8}$	$4.68 \cdot 10^{-8}$	2	2	1.5	0.3	0.05	0.2	X
Fuzzy-TP-PISF-CS	$6.33 \cdot 10^{-8}$	$6.6 \cdot 10^{-8}$	6	2	1.5	0.4	0.1	0.2	

Future research will be focused on the performance indices improvement by the design of CSs with adaptive nonlinear controllers and CSs with fractional order controllers (Folea et al., 2016), (Muresan et al., 2015) applied to mechatronics systems and by their fair comparison.

REFERENCES

[1] W. Wiboonjaroen and S. Sujitjorn, "Stabilization of a magnetic levitation control system via state-PI feedback," *Int. J. Mat. Mod. Meth.*, vol. 7, no. 7, pp. 717–727, Jul. 2013.

[2] M. B. Milovanovic´, D. S. Antic´, S. S. Nikolic´, S. Lj. Peric´, M. T. Milojkovic´, and M. D. Spasic´, "Neural network based on orthogonal polynomials applied in magnetic levitation system control," *Elektron. Elektrotech.*, vol. 23, no. 2, pp. 24–29, Jun. 2017.

[3] Z. Gong, L. Ding, H. Gao, H. Yue, R. Liu, and Z. Deng, "Design and control of a novel six-DOF maglev platform for positioning and vibration isolation," in *Proc. 2017 2nd Intl. Conf. Adv. Robot. Mech.*, Hefei, China, 2017, pp. 155–160.

[4] A. Rojas-Moreno and C. Cuevas-Condor, "Fractional order PID control of a MAGLEV system," in *Proc. Electron. Congr.*, Lima, Peru, 2017, pp. 1–4.

[5] A. Rojas-Moreno and C. Cuevas-Condor, "PD and PID control of a maglev system an experimental comparative study," in *Proc. 2017 IEEE 24th Intl. EEEC Conf.*, Cusco, Peru, 2017, pp. 1–4.

[6] K. M. Deliparaschos, K. Michali, and A. Zolotas, "On the issue of LQG embedded control realization in a Maglev system," in *Proc. 2017 25th Mediter. Conf. Control Autom.*, Valletta, Malta, 2017. pp. 1379–1384.

[7] H. Zhou, H. Deng, and J. Duan, "Hybrid fuzzy decoupling control for a precision maglev motion system," *IEEE/ASME Trans. Mechatron.*, vol. 32, no. 1, pp. 389–401, Feb. 2018.

[8] P. Baranyi, *TP-Model Transformation-Based-Control Design Frameworks*. Cham: Springer International Publishing, 2016.

[9] P. Galambos, J. Kuti, P. Baranyi, G. Szögi, and I. J. Rudas, "TP based convex polytopic modeling of nonlinear insulin-glucose dynamics," *in Proc. 2015 IEEE SMC Conf.*, Hong Kong, 2015, pp. 2597–2602.

[10] Y. Kunii, B. Solvang, G. Sziebig, and P. Korondi, "Tensor product transformation based friction model," in *Proc. 11th Intl. Conf. Intell. Eng. Syst.*, Budapest, Hungary, 2007, pp. 259–264.

[11] J. Matuško, V. Lešic´, F. Kolonic´, and Š. Ileš, "Tensor product based control of the single pendulum gantry process with stable neural network based friction compensation," in Proc. *2011 IEEE/ASME Intl. AIM Conf.*, Budapest, Hungary, 2011, pp. 1010–1015.

[12] B. Takarics and P. Baranyi, "Tensor-product-model-based control of a three degrees-of-freedom aeroelastic model," *J. Guid. Control Dyn.*, vol. 36, no. 5, pp. 1527–1533, Sep.–Oct. 2013.

[13] P. Korondi, "Tensor product model transformation-based sliding surface design," *Acta Pol Hung.*, vol. 3, no. 4, pp. 23–36, Dec. 2006.

[14] R.-E. Precup, S. Preitl, I.-B. Ursache, P. A. Clep, P. Baranyi, and J. K. Tar, "On the combination of tensor product and fuzzy models," in *Proc. IEEE Intl. AQTR Conf.*, Cluj-Napoca, Romania, 2008, vol. 2, pp. 48–53.

[15] P. Baranyi, P. Korondi, and K. Tanaka, "Parallel distributed compensation based stabilization of a 3-DOF RC helicopter: A tensor product transformation based approach," *J. Adv. Comput. Intell. Inform.*, vol. 13, no. 1, pp. 25–34, Mar. 2009.

[16] E.-L. Hedrea, C.-A. Bojan-Dragos, R.-E. Precup, R.-C. Roman, E. M. Petriu, and C. Hedrea, "Tensor product-based model transformation for position control of magnetic levitation systems," in *Proc. 26th Intl. Symp. Ind. Electron.*, Edinburgh, UK, 2017, pp. 1–6.

[17] E.-L. Hedrea, C.-A. Bojan-Dragos, R.-E. Precup, and T.-A. Teban, "Tensor product-based model transformation for level control of vertical three tank systems," in *Proc. 21st Intl. Conf. Intell. Eng. Syst.*, Larnaca, Cyprus, 2017, pp. 113–118.

[18] R.-E. Precup, L.-T. Dioanca, E. M. Petriu, M.-B. Radac, S. Preitl, and C.-A. Dragos, "Tensor product-based real time control of the liquid levels in a three tank system," in *Proc. 2010 IEEE/ASME Intl. AIM Conf.*, Montreal, Canada, 2010, pp. 768–773.

[19] R.-E. Precup, E. M. Petriu, M.-B. Radac, S. Preitl, L.-O. Fedorovici, and C.-A. Dragos, "Cascade control system-based cost effective combination of tensor product model transformation and fuzzy control," *Asian J. Control*, vol. 17, no. 2, pp. 381–391, Mar. 2015.

[20] C.-A. Bojan-Dragos, R.-E. Precup, S. Preitl, M.-B. Radac, D.-A. Matei, O. Tanasoiu, and E. M. Petriu, "Combined control solution for an advanced mechatronics application," in *Proc. 21st Intl. Conf. Syst. Theor. Control Comput.*, Sinaia, Romania, 2017, pp. 629–634.

[21] P. Baranyi, "TP model transformation as a way to LMI based controller design," *IEEE Trans. Ind. Electron.*, vol. 51, no. 2, pp. 387–400, Apr. 2004.

[22] R.-E. Precup, P. Angelov, B. S. J. Costa, and M. Sayed-Mouchaweh, "An overview on fault diagnosis and nature-inspired optimal control of industrial process applications," *Comp. Ind.*, vol. 74, pp. 75–94, Dec. 2015.